Molecular Dynamics Simulations of the Effects of Carbon Dioxide on the Interfacial Bonding of Polystyrene Thin Films

Coleman Alleman, Anand Srivastava, Somnath Ghosh

Computational Mechanics Research Laboratory, Department of Mechanical Engineering, The Ohio State University, Columbus, Ohio 43210

Correspondence to: S. Ghosh (E-mail: ghosh.5@osu.edu)

Received 1 March 2011; revised 12 May 2011; accepted 12 May 2011; published online 14 June 2011
DOI: 10.1002/polb.22288

ABSTRACT: Fabrication of nanoscale polymer-based devices, especially in biomedical applications, is a challenging process due to requirements of precise dimensions. Methods that involve elevated temperature or chemical adhesives are not practicable due to the fragility of the device components and associated deformation. To effectively fabricate devices for lab-on-a-chip or drug delivery applications, a process is required that permits bonding at low temperatures. The use of carbon dioxide (CO_2) to assist the bonding process shows promise in reaching this goal. It is now well established that CO_2 can be used to depress the glass transition temperature (T_g) of a polymer, allowing bonding to occur at lower temperatures. Furthermore, it has been shown that CO_2 can preferentially soften a polymer surface, which should allow for effective bonding at temperatures even below the bulk T_g. However, the impact of this effect on bonding has not been quantified, and the optimal bonding temperature and CO_2 pressure conditions are unknown. In this study, a molecular dynamics model is used to examine the atomic scale behavior of polystyrene in an effort to develop understanding of the physical mechanisms of bonding and to quantify how the process is impacted by CO_2. The final result is the identification of a range of CO_2 pressure conditions which produce the strongest bonding between PS thin films at room temperature. © 2011 Wiley Periodicals, Inc. J Polym Sci Part B: Polym Phys 49: 1183–1194, 2011

KEYWORDS: adhesion; carbon dioxide; decohesion; interfaces; mechanical properties; molecular dynamics; polystyrene; surfaces; thin films

INTRODUCTION Polymer bonding at the nanoscale is a critically important part of the processing and fabrication of biomedical nanodevices for lab-on-a-chip and drug delivery applications. Conventional techniques such as welding at elevated temperatures or using chemical adhesives may not be practicable for two reasons:

1. The required precision of the geometric features in the devices is destroyed;
2. Biomolecules implanted in the polymer surfaces cannot survive excessive heat or harsh chemicals.

Carbon dioxide (CO_2) assisted bonding techniques are being developed to yield a process that is biologically benign and that preserves nanoscale features. Experimental setups like the one schematically depicted in Figure 1 are being used to study the impact of macroscopic variables like time, temperature, CO_2 pressure, and applied force on the development of adhesive strength during the CO_2 assisted bonding process.[1] Parallel experimental efforts are being made to understand the nanoscale properties that govern the effectiveness of various processing conditions,[2] but a limited understanding of the process at the nanoscale is still a barrier to fabrication. In this study, molecular dynamics (MD) is used to access information about material behavior at the atomic level, thereby providing quantitative analysis of some of the fundamental mechanisms of the bonding process.

The CO_2 assisted bonding process relies on the plasticization of the polymer to allow diffusion of chain segments across the bonding interface. A substantial body of experimental, theoretical, and simulation work[3–6] has established that CO_2 is able to depress the bulk glass transition temperature or T_g^b of polystyrene (PS) by as much as 65 °C. This phenomenon effectively plasticizes the polymer at lower temperatures. The softening is characterized by heightened chain mobility and increased free volume.[6,7] It has also been established that there exists a surface region in PS thin films where molecules undergo the glass transition at an even lower surface glass transition temperatures.[8,9] These two effects can be effectively utilized to bond polymeric nanodevices at near room temperatures in the presence of CO_2, while maintaining precise geometries and dimensionalities of the constituents.

Adhesive strength at a symmetric polymer-polymer interface is known to depend on the amount of diffusion across the bonding interface.[10] As this diffusion process takes place, a

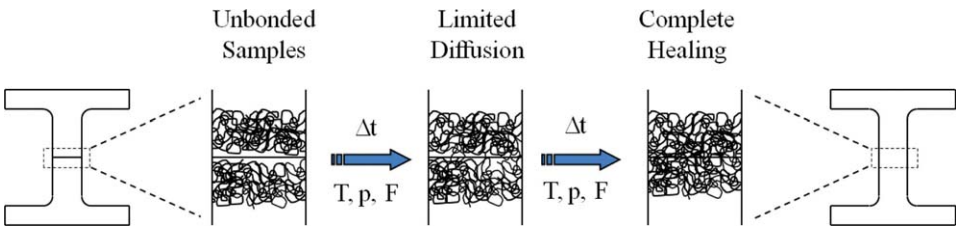

FIGURE 1 Schematic representation of an experimental setup for the CO_2 assisted bonding process in PS thin films for fabricating nanoscale devices.

region develops where atoms from both sides persist. This process has been extensively studied and accurately quantified by both experimental means[11,12] and through simulations.[13–15] It has been shown in previous studies that the strength of the adhesion at the interface is dependent on the width of this region.[16–18] The rate of diffusion depends on the temperature, external force and the amount of time elapsed.[19] This study shows that gas sorption as a result of processing in a CO_2 environment also impacts diffusion, increasing the amount of diffusion that occurs across the interfacebetween two polymer thin films.

The adhesive strength at symmetric PS–PS interfaces has been examined in a number of experimental studies using various methods including T-peel tests and lap-shear tests.[20–23] At the atomic level, adhesive strength is dependent on the proximity of atoms from molecules on opposite sides of the interface. Beyond a threshold amount of atomic separation, the attractive forces due to nonbonded interactions are insufficient to cause adhesion between opposing atomic surfaces at the interface. This paper presents a novel computational method for evaluating adhesive strength via MD modeling of deformation and decohesion. This method, which captures data at finer scales than is possible with current experimental techniques, allows investigation of the nanoscale mechanisms at work during the macroscopic processes of bonding and bonding interface decohesion.

The present MD-based study shows that the introduction of CO_2 increases the local separation between the film surfaces on either side of the interface. This phenomenon reduces the adhesive strength of the interface due to the increase in free volume at the interface that is driven by absorption of CO_2. Results of the MD simulations conclude that the addition of CO_2 molecules into the bonding process produces a competition between one mechanism that serves to facilitate the bonding process and another that hinders it. This suggests that there exists an optimal amount of CO_2 that when introduced into the polymer system will produce the best bonding. This optimal amount of CO_2 is assessed in this study by examining the functional relationship between bond strength and the amount of CO_2 present during bonding.

MODEL DEVELOPMENT AND SIMULATION PROCEDURES

Overview of Modeling Scheme

Molecular dynamics models of binary PS-CO_2 systems are simulated for understanding the operating atomic-scale mechanisms during CO_2 assisted polymer bonding. Each system consists of two PS thin films containing a prescribed number of molecules in a CO_2 environment. The system is subjected to a controlled pressure environment that is applied in the non-periodic thickness direction by repulsive walls. A representative molecular system for this simulation setup is shown in Figure 2. Simulations are carried out in a three-stage process. In the first stage, the initial configurations are created and equilibrated via methods previously described.[6,24] These include separate procedures for pure PS, pure CO_2, and binary PS-CO_2 systems. After equilibration of each component separately and subsequent equilibration of the full binary system, the bonding process is simulated. Lastly, the CO_2 is eliminated, and simulations are carried out to test the integrity of the bonded interfaces under tensile loading. All simulations are carried out with the LAMMPS software package, with an NVT ensemble implementing a Nose/Hoover thermostat set to 300 K with a relaxation time of 10 fs.

Modeling Polystyrene: Potential Functions and Equilibration Procedure

The simulated polymer is monodisperse atactic PS with 200 monomers per chain molecule. This results in a molecular weight of $M_W = 21$ kg/mol. This low molecular weight is chosen in order to create a model system wherein the relevant chain dynamics happen on a fast timescale while retaining a close correspondence to a useful physical material. For example, $M_W = 21$ kg/mol is well below the critical entanglement molecular weight for PS, $M_{ce} = 36$ kg/mol,[21] thus avoiding the effects of chain entanglement that are expected to show up only on much longer time scales than those investigated here.[25] Also, a low molecular weight is advantageous for MD study, since the time required for bonding has been found to depend strongly on chain length.[26,27] Two film sizes are simulated in this study. They contain 10 and 15 chain molecules each, respectively denoted as "10 × 200" and "15 × 200". The PS chains are assembled in the form of freestanding thin films, with periodic boundaries imposed in the two horizontal directions of the cross-section. Nonperiodic, finite boundary conditions are enforced in the vertical thickness direction. The PS molecules are assembled using the augmented Phantom Chain Growth (PCG) scheme that has been developed by the authors.[24] Additional monomers are introduced in the PCG model based on a predetermined conditional probability. In this algorithm, monomers are introduced based on sampling of a random distribution of the backbone dihedral angle. The total energy change ΔU resulting from the introduction of a

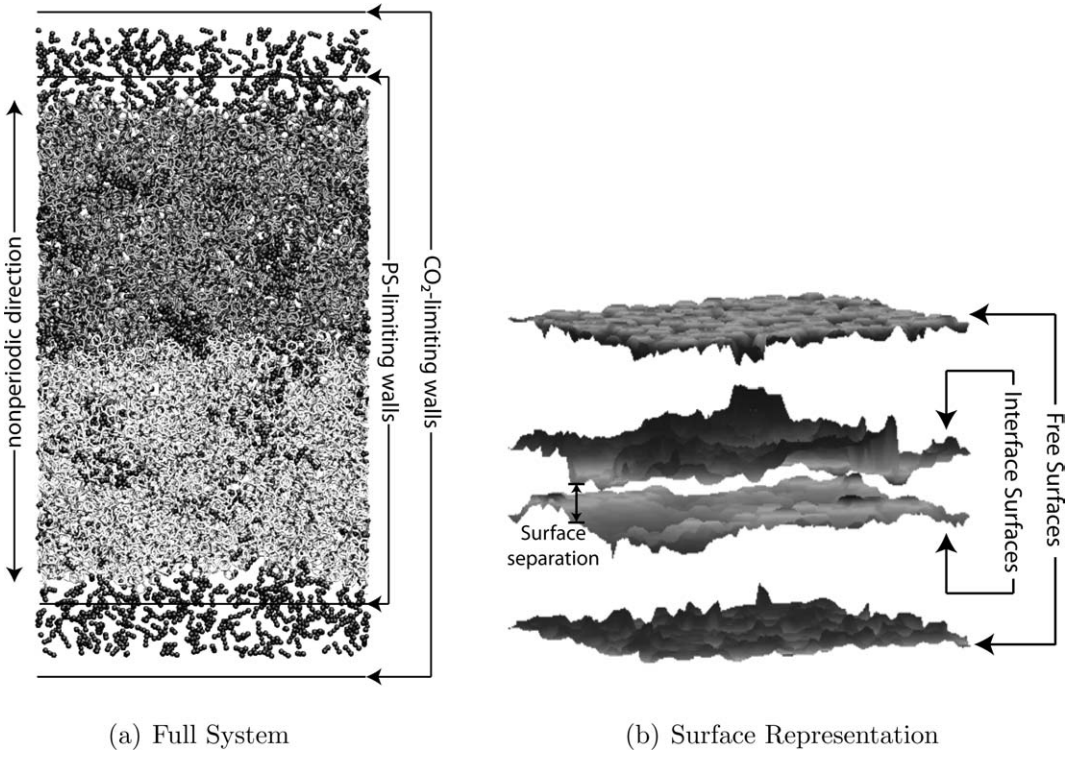

FIGURE 2 A molecular simulation system for the thin film bonding process: (a) The full MD representation of the PS thin films and CO_2 with the films shaded differently for identification, (b) The surfaces of the PS thin films are represented by an interpolation of the van der Waals surfaces as used for the measurement of film separation.

new site is calculated as the sum of the dihedral and non-bonded interactions. The probability of the acceptance of the new monomer is expressed as:

$$p = \min[1, \exp(-\beta \Delta U)] \tag{1}$$

where β is the reciprocal of the product of the Boltzmann constant k_B and the temperature of the system. If after a certain number of trials, the new monomer segment is not acceptable, the chain is shortened by a single segment and the entire procedure is repeated with another dihedral angle. In the direction of the film thickness, an additional penalty potential function U_p is imposed to contain the growing chains. This potential energy function is given as:

$$U_p(d) = \epsilon_b \left(\frac{\sigma_b}{d}\right)^{12} \tag{2}$$

where d is the distance to the prescribed simulation boundary, and $\epsilon_b = 10$ kcal/mol and $\sigma_b = 5$ Å are empirically determined Lennard-Jones (LJ) parameters. For a monomer to be added to a growing chain, the condition $U_p < U_{tol}$ must be satisfied.

The potential functions governing the interactions of the PS united atoms are adapted from the work of Wick et al.[28] and previously employed by Harmandaris et al.,[29] with the exception of using a harmonic bond potential. The total potential energy for PS is given by

$$U_{PS} = \frac{1}{2}k_B(r - r_0)^2 + \frac{1}{2}k_\theta(\theta - \theta_0)^2 + \frac{1}{2}\sum_{j=1}^{3} k_\phi^j \cos[1 + (-1)^{j+1} j\phi] + \frac{1}{2}k_\psi(\psi - \psi_0)^2 + 4\epsilon_{ij}\left[\left(\frac{\sigma_{ij}}{r_{ij}}\right)^{12} - \left(\frac{\sigma_{ij}}{r_{ij}}\right)^{6}\right] \tag{3}$$

The parameter values for the bond stretch energy are taken from Han and Boyd[30] and are given in Table 1. Actual values from spectroscopy are used for the parameters.

After chain creation, the films are equilibrated at 500 K and then cooled to 300 K over a simulation time of 6 ns. Equilibration takes place in a simulation volume measuring 8 nm by 8 nm in the two periodic directions of the cross-section. At the end of the equilibration phase, the height of the film in the 10×200 system is approximately 5 nm and the height of the 15×200 film is 7 nm.

Modeling Carbon Dioxide: Potential Functions and Equilibration Procedure

For CO_2, the EPM2 model developed by Harris and Yung[31] is used with a harmonic flexible bond potential. The total interatomic potential function for CO_2 is given as:

$$U_{CO_2} = \frac{1}{2}k_B(r - r_0)^2 + \frac{1}{2}k_\theta(\theta - \theta_0)^2 + \frac{q_i q_j}{4\pi\varepsilon_0 r_{ij}} + 4\epsilon_{ij}\left[\left(\frac{\sigma_{ij}}{r_{ij}}\right)^{12} - \left(\frac{\sigma_{ij}}{r_{ij}}\right)^{6}\right] \tag{4}$$

TABLE 1 Parameter Values (Energies in kcal/mol) in the Potential Energy Functions for PS

Bond Stretch Parameters			
Bond type		k_B	r_0 (Å)
CH_x-CH		316.92	1.54
CH-C_{aro}		316.92	1.51
$C(H)_{aro}$-CH_{aro}		525.81	1.40
Bond angle parameters			
Bond type		k_θ	θ_0 (°)
CH_3-CH-CH_2		62.14	112
CH-CH_2-CH		62.14	114
$C(H)_{aro}$-$C(H)_{aro}$-$CH_{(aro)}$		119.50	120
Bond torsion parameters			
Bond type	k_ϕ^1	k_ϕ^2	k_ϕ^3
CH_x-CH-CH_2-CH	1.41	−0.27	3.14
Bond improper dihedral parameters			
Bond type		k_ψ	ψ_0 (°)
$C(H)_{aro}$-CH_{aro}-CH_{aro}-CH_{aro}		20.00	0
CH-CH_x-CH_y-C_{aro}		40.01	35.26
LJ pair potential parameters			
Interaction type		ε	σ (Å)
CH_3-CH_3		0.1950	3.750
CH_2-CH_2		0.0915	3.950
CH-CH		0.0199	4.650
C_{aro}-C_{aro}		0.1003	3.695
CH_{aro}-CH_{aro}	23	0.0596	3.700

The mixed LJ parameters are calculated via the Lorentz-Berthelot mixing rule.[34]

where the values of the parameters are given in Table 2. For a given simulation volume, the number of CO_2 molecules is determined by solving and inverse problem for the van der Waals equation of state for a target pressure. The target CO_2 pressures in this study are: 0.0 (absence of CO_2), 0.7, 1.4, 2.8, and 5.5 MPa, respectively. This corresponds to the range of pressures that has been considered in the experimental studies of Ellis et al.[1] and Yang et al.[2] The pressures reported in the results are the CO_2 virial pressures developed in the combined PS-CO_2 systems. These differ from the target pressures achieved in the pure CO_2 systems mainly due to the volume exclusion of the PS. The CO_2 molecules are initially positioned in simulation volumes with the same dimensions as the PS volumes via an algorithm that minimizes the total potential energy, which is the sum of that due to the repulsive part of the LJ pair interactions and the energetic penalty potential U_p. The nonperiodic boundaries in the thickness direction are maintained by employing a LJ-type wall interaction given by

$$U_{\text{boundary}}(r) = 4\epsilon_b\left[\left(\frac{\sigma_b}{r}\right)^{12} - \left(\frac{\sigma_b}{r}\right)^{6}\right], \qquad r \le 2^{1/6}\sigma_b \tag{5}$$

Parameters ϵ_b and σ_b are determined empirically and set at 10 kcal/mol and 5 Å, respectively. The cutoff is set to include only repulsive interaction while eliminating force discontinuity at the cutoff. Following the initial positioning, the pure CO_2 systems are brought to equilibrium at 300 K during an equilibration phase of 100 ps.

Modeling the PS-CO_2 Binary Systems: Potential Parameters and Equilibration Procedure

To equilibrate the binary systems before the bonding simulation, two identical simulation volumes, each containing an equilibrated freestanding PS thin film are interfaced after translating each film in the nonperiodic thickness direction by $\pm(h/2 + 0.2\,\text{nm})$, h being the film height. This creates a simulation volume containing two identical freestanding films separated by a gap of at least 0.4 nm in the thickness direction. The two-film configuration is then re-equilibrated over 100 ps to create a symmetric PS–PS interface. At the end of this equilibration, the gap between the films is reduced significantly due to movement of the film mass centers, but the interface between the two films is readily identifiable by a marked drop in PS density.

A simulation volume containing the equilibrated CO_2 sample is then superimposed on the two-film volume to create the full PS-CO_2 binary system. A soft potential, given in the LAMMPS literature[32]

$$E(r_{ij}) = A\left[1 + \cos\left(\frac{\pi r_{ij}}{r_c}\right)\right] \qquad r_{ij} < r_c \tag{6}$$

is initially used between PS and CO_2 to eliminate any excessive forces due to the physically unrealistic overlap that may initially occur between the atoms. The system trajectories are evolved over a short simulation period of 10 ps in preparation for the bonding simulations.

For the remaining simulations, a full LJ potential is implemented between PS and CO_2 atoms. The potential parameters are determined using the mixing rule that has been developed

TABLE 2 Parameter Values (Energies in kcal/mol) in the Potential Energy Functions for CO_2

Bond Stretch Parameters		
Bond type	k_B	r_0 [Å]
C=O	557.45	1.149
Bond angle parameters		
Bond type	k_θ	θ_0 [°]
O=C=O	147.71	180
Coulombic interaction parameters		
Atom type	q [e]	
O	−0.3256	
C	+0.6512	
LJ pair potential parameters		
Interaction type	ε	σ [Å]
O-O	0.1937	3.033
C-C	0.1228	2.757
C-O	0.1542	2.892

The mixed LJ parameters are calculated via the Lorentz-Berthelot mixing rule.

TABLE 3 Mixed LJ Parameters for PS-CO_2 Interaction Calculated via the Halgren Mixing Rule

LJ Pair Potential Parameters			
Atom type		ε	σ
CH_3	O	0.1944	3.4665
CH_2	O	0.1286	3.6099
CH	O	0.0456	4.1674
C_{aro}	O	0.1357	3.4285
CH_{aro}	O	0.0986	3.4319
CH_3	C	0.1527	3.4016
CH_2	C	0.1054	3.5592
CH	C	0.0404	4.1576
C_{aro}	C	0.1107	3.3595
CH_{aro}	C	0.0828	3.3633

Energies are in kcal/mol and distances are in angstroms.

in Srivastava et al.[6] This mixing rule determines the values of the LJ parameters via the formulae given in Halgren[33]

$$\sigma_{ij} = \frac{\sigma_{ii}^3 + \sigma_{jj}^3}{\sigma_{ii}^2 + \sigma_{jj}^2}, \quad \epsilon_{ij} = \frac{4\epsilon_{ii}\epsilon_{jj}}{\left(\epsilon_{ii}^{1/2} + \epsilon_{jj}^{1/2}\right)^2} \tag{7}$$

where the ith atom is from a CO_2 molecule, and the jth atom is from a PS molecule. Parameter values calculated by this mixing rule are given in Table 3. As detailed in Srivastava et al.,[6] this mixing rule is implemented for interactions between dissimilar species for its ability to produce experimentally observed free volume characteristics better than the commonly used Lorentz-Berthelot rule.[34]

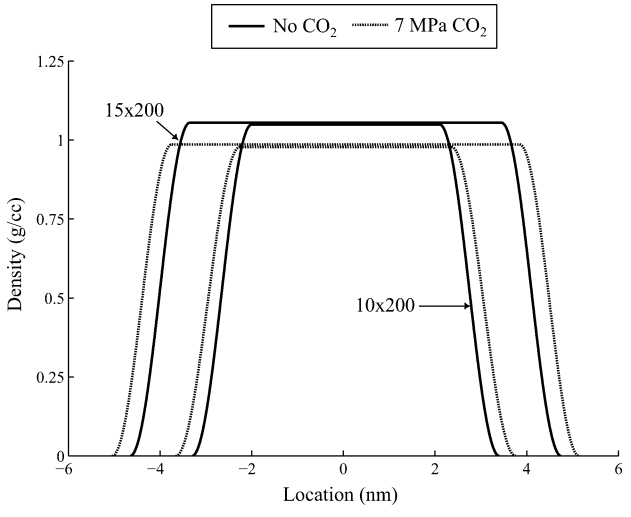

FIGURE 3 Polystyrene density along the nonperiodic thickness direction for a single freestanding film. To highlight the change in profiles upon addition of CO_2, the plotted curves are obtained by fitting smooth curves to the surface region densities and the average core densities.

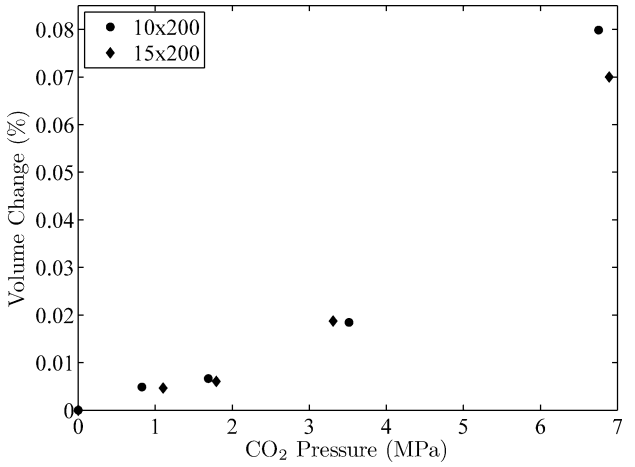

FIGURE 4 Percentage volume change for two PS thin film under various CO_2 pressure conditions (zero pressure corresponds to absence of CO_2). Error is of the order of the marker size.

INVESTIGATION OF THIN FILM BEHAVIOR: MODEL VALIDATION AND PRELIMINARY STUDY

Film Density Characteristics

Prior to modeling the actual interface bonding process, a study of the thin film characteristics is performed to validate parameters in the potential functions and the overall simulation setup. The thin film model for PS is first validated by comparing density at the film core to the experimental value of 1.05 g/cm^3 reported in Wissinger and Paulitis.[35] As shown in Figure 3, the simulation values for both films of pure PS are within 1% of the experimental value. Near the film surfaces, however, there exists a gradient in the density. The extent of this surface region is roughly constant for the two film heights studied. The addition of CO_2 extends this region somewhat, for reasons discussed below. In addition, CO_2 causes an expansion in the PS at the film core. This expansion is quantified in terms of the change in volume for the pure PS system shown in Figure 4. The agreement with the experimental data of Wissinger and Paulitis[35] confirm the accuracy of the MD simulation model in predicting swelling due to the presence of CO_2.

Chain Dynamics in the Thin Films

In addition to the variation in surface density characteristics, the efficacy of bonding is determined in large part by the chain dynamics that take place at the bonding interface. Significant studies have been conducted on the surface dynamics of thin PS films. It has been argued by Kawaguchi et al.[36] that there exists a gradient in mobility across the thickness of the film. Kawana and Jones[37] have demonstrated that there exists a liquid-like surface layer that persists below the glass transition temperature. The computational methods used in this study allow the investigation of surface dynamics at atomic resolution and in the absence of the substrate effects that are necessarily present in any experimental study. To quantify the deviation in mobility found near the film surface, a relative measure of MSD is defined as:

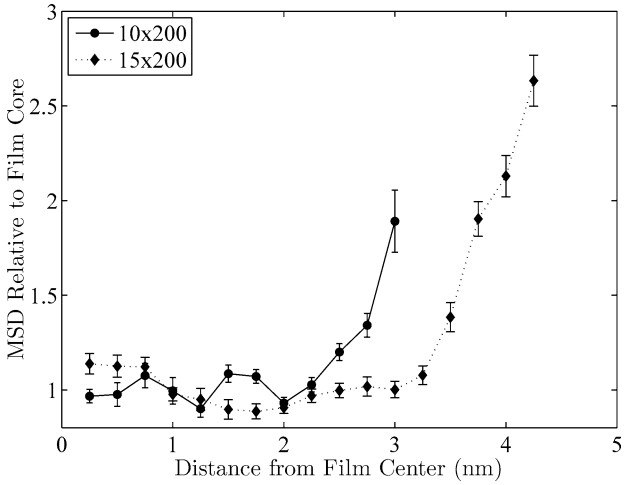

FIGURE 5 Layer-wise mobility, MSD_{rel}, for polymer atoms in a thin film. Error bars represent the standard deviation in the measurement.

$$MSD_{rel} = MSD_{layer}/MSD_{core} \quad (8)$$

where MSD_{layer} corresponds to the mean squared displacement for atoms in a given layer, and MSD_{core} is averaged over atoms in all layers from the center of the film, where there is no layer-wise gradient in mobility. As shown in Figure 5, the model in this study is able to quantify the effect of the free surface on mobility. It shows that an enhancement in the mobility extends ~1 nm into the film. This effect contributes to a two to three fold increase in the mobility of atoms near a free surface in comparison with those in the film cores. This is in agreement with the measurements presented in the work by Baljon et al.[38] This increase in mobility at the free surface is not present at the film–film interface during bonding. However, as discussed below, the addition of CO_2 can similarly increase the mobility at the bonding interface, causing the film surfaces there to behave more like free surfaces.

NUMERICAL EXPERIMENTS ON THE BONDING PROCESS

Simulation of Bonding in PS-CO_2 Binary Systems

As described by Prager and Tirrell,[39] bonding at a symmetric polymer-polymer interface is brought about as the interface heals, eventually becoming indistinguishable from the rest of the material. During this healing process, the adhesive strength of the interface gradually grows as the material surfaces on opposite sides of the interface rearrange and the discontinuities in the material properties that define the interface are eliminated. In this study, three mechanisms of healing are identified and quantified in the initial part of the bonding process. First, the discontinuity in material density at the interface is eliminated as the film surfaces rearrange to conform more closely to one another. Second, groups of atoms near the film surfaces start to diffuse across the boundary and the interface between molecules of different films begins to resemble the interface between molecules within a film. Third, chain segments from molecules belonging to one film begin to penetrate into the space occupied by molecules of the opposite film. The numerical experiments performed in this study are designed to study these mechanisms under various CO_2 pressure conditions in terms of their impact on interfacial adhesive strength.

Using procedures described above, simulations of the bonding process are carried out for ten model systems, corresponding to two film heights and five CO_2 pressure conditions. The simulations are conducted at a constant temperature of 300 K for a period of 3 ns with a timestep of 3 fs. This simulation time is orders of magnitude lower than the experimental times, during which Fickian diffusion has been identified as a main driver of the development of interfacial adhesive strength. Thus, the simulations presented here attempt to identify the mechanisms at work during the initial healing of the interface at times shorter than the Rouse time.[40] Additionally, longer simulations of 33 ns are carried out for two systems of interest in order to analyze the time-dependence of some of the important results. During the simulations, statistical data is collected and subsequently analyzed using the procedures detailed in the remainder of this section in order to provide a comprehensive quantification of the atomic behavior critical to the development of adhesive strength at the bonding interfaces.

Density Profiles and Diffusion at the Interface

At the outset of the bonding process, the material discontinuity between the two polymer surfaces at the interface is the most obvious obstacle to the development of interfacial strength. For PS at 300 K, the timescale of MD simulation is such that bulk diffusion does not occur at a significant level within the available sampling window. However, the simulated surfaces are much smoother than a typical experimental sample, due to the small surface area and regularity resulting from the careful equilibration of the individual films. This results in the rapid elimination of the discontinuity in the density of the polymer at the interface during the simulation. Figure 6

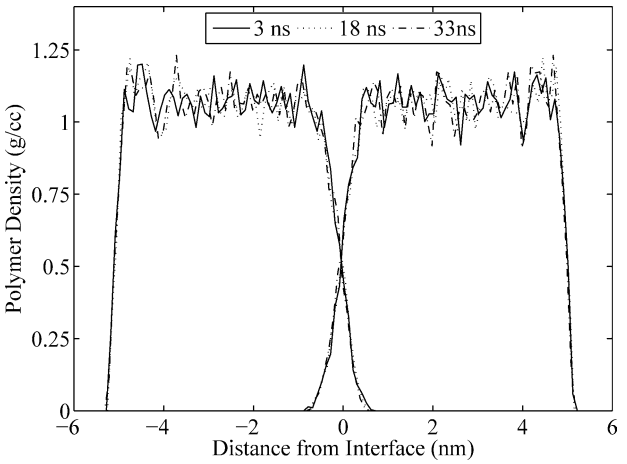

FIGURE 6 Polystyrene density along the nonperiodic thickness direction for two 10 × 200 films with 1.7 MPa CO_2 pressure at several times during a bonding simulation.

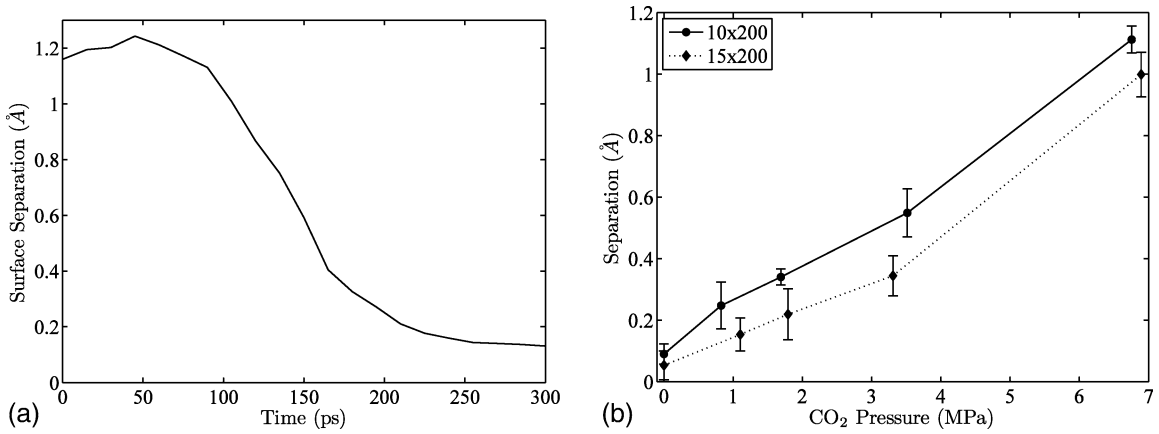

FIGURE 7 (a) Example of the measurement of surface separation at the interface versus time using the 15 chain molecule, 200 psi PS-CO_2 system; (b) Equilibrium surface separation S_0 at the interface following 3 ns of simulation time as a function of CO_2 pressure. Error bars represent the standard deviation in the measurement.

plots the polymer density across the thickness direction of two films during a bonding simulation. As shown in this figure, the deviation in material density from point to point across the thickness obscures time-dependent change in the density at any given point. Additionally, the interfacial width—as measured by the density—does not appear to widen appreciably over the MD timescale. Thus, it is necessary to introduce additional measures to analyze the persistence of the interface.

A small, localized separation between the surfaces of the films persists at the interface even after the density stabilizes. To identify this material discontinuity, the local separation between atomic surfaces of the films at the interface is measured by calculating the perpendicular distance between the van der Waals surfaces of surface atoms in opposite films over a square grid with resolution 1 Å. A mean value is obtained by averaging the separation at each grid point.

During the bonding simulation, the mean surface separation rapidly decreases and subsequently stabilizes to roughly its final value at times ~300 ps. This is depicted in Figure 7(a). The curve is typical of all simulation systems, except that the equilibrium separation S_0 depends on CO_2 pressure, as seen in Figure 7(b). In Figure 7(b), the final separation between the film surfaces increases with increasing CO_2 pressure. Thus, according to this measure, the interface becomes more pronounced with increasing CO_2 pressure. This phenomenon indicates that at least one effect introduced by the presence of CO_2 serves to degrade adhesive strength. However, the mean separation does not change appreciably over time after the initial 300 ps of the simulation, while the strength of the bonded interface continues to develop up to experimental timescales. This suggests that there are additional factors contributing to the development of adhesive strength at the interface.

Although the variation in density across the film thickness partially obscures changes at the interface, it is possible to measure the rearrangement of the structure of the film surfaces at the interface. The diffusion of chain segments across the interface between the upper and lower thin films is quantified using the average monomer inter-penetration depth $X(t)$, given by

$$X(t) = \frac{\int_{z=0}^{\infty} z(t)C(z,t)dz}{\int_{z=0}^{\infty} C(z,t)dz} \tag{9}$$

where $C(z,t)$ is the monomer concentration profile and $z(t)$ is the distance from a diffusing monomer back to the interface, as discussed by Wool.[25] For the discrete atomistic system, this measure is calculated as

$$X(t) = \frac{\sum_{i=1}^{N} z_i(t)m_i}{2\sum_{i=1}^{N} m_i} \tag{10}$$

where N is the number of atoms that have crossed the interface, and m_i is the atomic mass of the i-th atom. The factor of $1/2$ is added to account for the symmetric nature of the films across the interface. In Figure 8, data from the shorter 3 ns simulations are shown for all systems, as well as values from the two extended 33 ns simulations of the 10×200 systems without CO_2 and with 1.7 MPa CO_2. As seen in this figure, the value of the interpenetration depth increases with increasing CO_2 pressure for both film sizes. Contrary to the trend seen in the mean separation between the atomic surfaces at the interface, this measure suggests that the bonded interface becomes stronger with increasing CO_2 pressure. Additionally, the measured values of the inter-penetration depth are shown to increase appreciably for the longer 33 ns simulations, indicating that a stronger interface should be observed for the resulting systems. Thus, it is seen that diffusion at the interface is measurably affected upon introduction of CO_2 into the system. However, the overall impact on the development of adhesive strength is not clearly elucidated by these simple measurements.

Free Volume Characteristics and Chain Bridging at the Interface

To further investigate the atomic structure of film surfaces at the bonding interface, two additional measures are introduced.

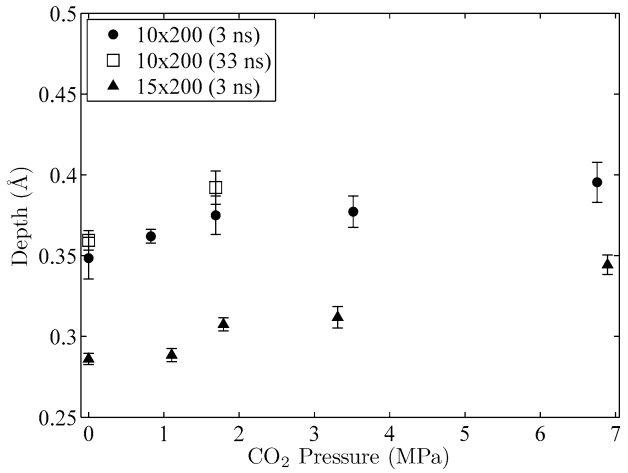

FIGURE 8 Average monomer inter-penetration as a function of CO_2 pressure for two different timescales and film thicknesses. Error bars represent the standard deviation in the measurement.

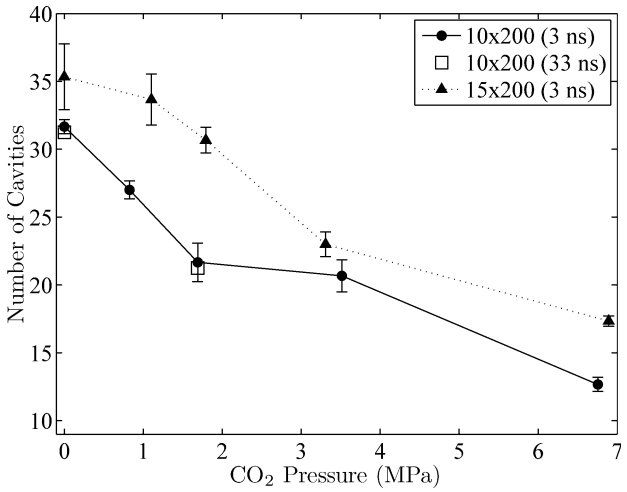

FIGURE 9 Average number of cavities at the interface as a function of CO_2 pressure for two different timescales and film thicknesses. Error bars represent the standard deviation in the measurement (for the 33 ns simulations, the error is smaller than the marker size). Lines are a guide to the eye.

First, the free volume at the surface is characterized in terms of the number and average size of cavities at the interface. A cavity is assumed to be a contiguous set of grid points where the separation between film surfaces is greater than 1 Å. The cavity volume is calculated as as discrete sum, expressed as:

$$V_C = A \sum_{i=1}^{N} h_i \tag{11}$$

where A is the area of a grid square, N is the number of grid squares occupied by the cavity, and h_i is the separation between the film surfaces at the grid square. In Figures 9 and 10 free volume data from the shorter 3 ns simulations are shown for all systems, as well as values from the two extended 33 ns simulations of the 10×200 systems without CO_2 and with 1.7 MPa CO_2. As seen in these figures, the number of cavities decreases while their mean sizes increase with increasing CO_2 pressure. It is also noted that the changes in the cavity number and volume values plotted in Figures 9 and 10 are not statistically significant for the extended 33 ns simulations, indicating that the free volume characteristics do not contribute significantly to any changes observed in the systems resulting from the longer simulation time. The combined effect of these two trends results in an increasing free volume with increasing CO_2 pressure. This is the main contributor to the mean surface separation trend, detailed above. With this information, it is possible to reconcile the opposing trends in diffusion observed above. On the one hand, CO_2 plasticizes the polymer, enhancing diffusion across the interface. At the same time, pockets of adsorbed CO_2 on the film surfaces merge and persist, inhibiting close surface contact and increasing the mean surface separation.

Next, the number of chain segments that bridge the interface is considered. The existence of a bridging segment is identified by a contiguous set of grid points over which the penetration of a chain of atoms from one film into the other is greater than the van der Waals radius of the PS united atoms. In Figure 11, the numbers of chain bridges measured in the shorter 3 ns simulations are shown for all systems, as well as values from the two extended 33 ns simulations of the 10×200 systems without CO_2 and with 1.7 MPa CO_2. The figure illustrates a remarkable trend in the number of bridges. This value increases with the CO_2 pressure, reaches a maximum at $\sim$2 MPa, and subsequently decreases with further pressure elevation. The attainment of the plotted values occurs in the first few nanoseconds of the simulations, and the values do not change in a statistically significant way beyond 3 ns for the two extended simulations. Thus, the development of chain bridges does not contribute significantly to any changes

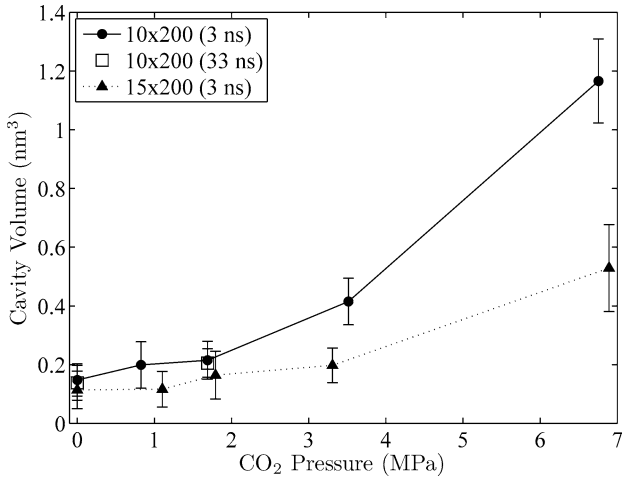

FIGURE 10 Average volume of cavities at the interface as a function of CO_2 pressure for two different timescales and film thicknesses. Error bars represent the standard deviation in the measurement. Lines are a guide to the eye.

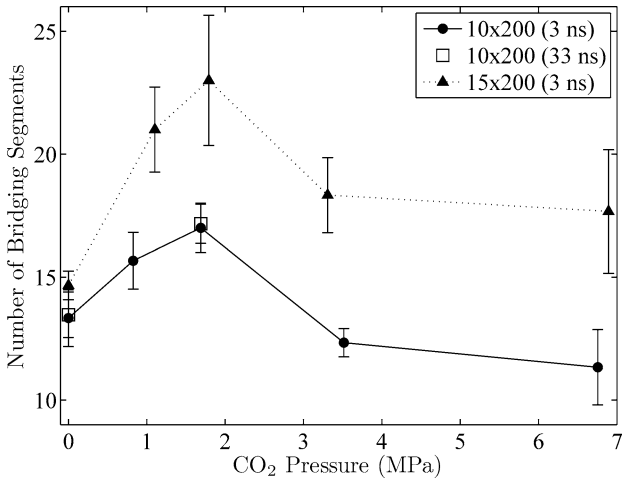

FIGURE 11 Number of chain segments bridging the interface as a function of CO_2 pressure for two different timescales and film thicknesses. Error bars represent the standard deviation in the measurement. Lines are a guide to the eye.

observed in the systems resulting from the longer 33 ns simulation times. Of the measurements discussed thus far, this is the first quantity directly related to strength development that has a maximum at a finite CO_2 pressure. The goal of the remainder of this section is to identify a dynamic mechanism that can explain why this maximum is observed.

Dynamic Behavior of Chains at the Interface

A study of the dynamic behavior of atoms at the bonding interface sheds light on the trend in the development of bridging chain segments. The mean-squared displacement for atoms at the interface is measured as

$$MSD = \langle |\vec{x}(t) - \vec{x}(0)|^2 \rangle \tag{12}$$

where $\vec{x}(t)$ and $\vec{x}(0)$ correspond to the positions of the atoms at time $= t$ and time $= 0$, respectively. The data is gathered over a period of 200 ps during the bonding process simulations. In a volume with a height of 1 nm centered at the interface, the mobility of atoms is found to increase with CO_2 pressure up to a maximum at $\sim$2 MPa. Increasing the CO_2 pressure beyond this begins to limit mobility, as shown in Figure 12, where MSD data is collected and averaged over the last 2 ns of the simulation of bonding. Thus, for a particular range of CO_2 pressures, the mobility at the interfacial surfaces can be enhanced in a manner similar to that observed at the free surfaces studied. This trend is similar to that found in the number of bridges being developed. This infers that an increase in mobility promotes chain bridging.

Simulation of Interface Decohesion

After the simulations of the initial phase of the bonding process, simulations are performed to test the adhesive strength of the PS interfaces. At the outset of these simulations, interactions between PS and CO_2 atoms are turned off, and the systems are allowed to relax for a simulation period of 50 ps to mitigate the residual stresses induced by the termination of the PS-CO_2 interactions. A layer of atoms 1 nm thick is frozen at the edges of the films away from the interface in the non-periodic thickness direction. These atoms are then displaced with a uniform velocity to keep the effective engineering strain rate at $\dot{e} = 2e8\,s^{-1}$. This rate is chosen for computational efficiency after performing a sensitivity study to determine the dependence of strain energy density on the strain rate. In simulations employing a strain rate of $\dot{e} = 2e9\,s^{-1}$, the strain energy developed is 18% higher than the value obtained for $\dot{e} = 2e8\,s^{-1}$. However at a lower rate of $\dot{e} = 2e7\,s^{-1}$, the strain energy measurement is within 1% of the value obtained at $\dot{e} = 2e8\,s^{-1}$. The films are strained until the interface fails, over a period of around 0.5 ns, with decohesion occurring at $\epsilon_f \approx 6\%$. This is shown in Figure 13, which plots the stress-strain curve for each system as it undergoes the process of decohesion. In every system simulated, the films separate completely, with decohesion occurring at the original interface.

Interface Integrity: A Strain Energy Density Based Metric

The importance of the chain bridging and mobility data is demonstrated by the measurement of integrity of the interface that has developed during the simulation of bonding. To measure this integrity, the stress is calculated for a collection of atoms initially contained in a volume including the entire cross-section perpendicular to the thickness direction and spanning 2 nm around the interface in the thickness direction. The stress tensor is calculated from the sum of the local atomic virial stresses as[41,42]

$$\boldsymbol{\sigma} = \frac{1}{V}\sum_i \left[\frac{1}{2}\sum_{j\neq i}\left(\vec{r}_{ij} \otimes \frac{\partial \Phi}{\partial r_{ij}} \frac{\vec{r}_{ij}}{\|\vec{r}_{ij}\|} \right) - m_i \vec{v}_i \otimes \vec{v}_i \right] \tag{13}$$

Here, $\vec{r}_{ij}$ is the vector from the position of the i-th atom to the position of the j-th atom. The velocity $\vec{v}_i$ is the total velocity vector of the i-th atom less the contribution due to the

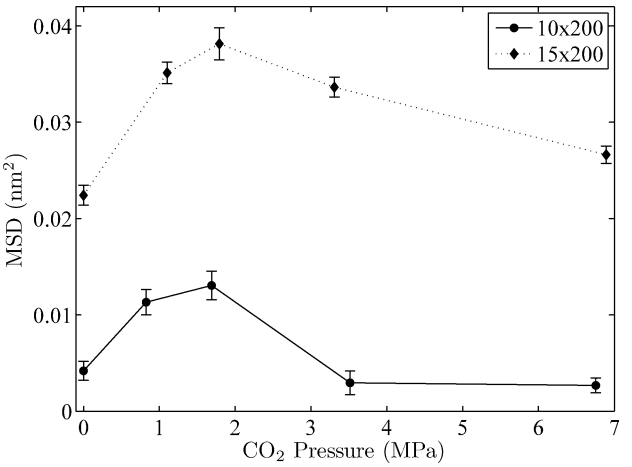

FIGURE 12 Mean-squared displacement for atoms in the interface region over 200 ps as a function of CO_2 pressure. Error bars represent the standard deviation in the measurement.

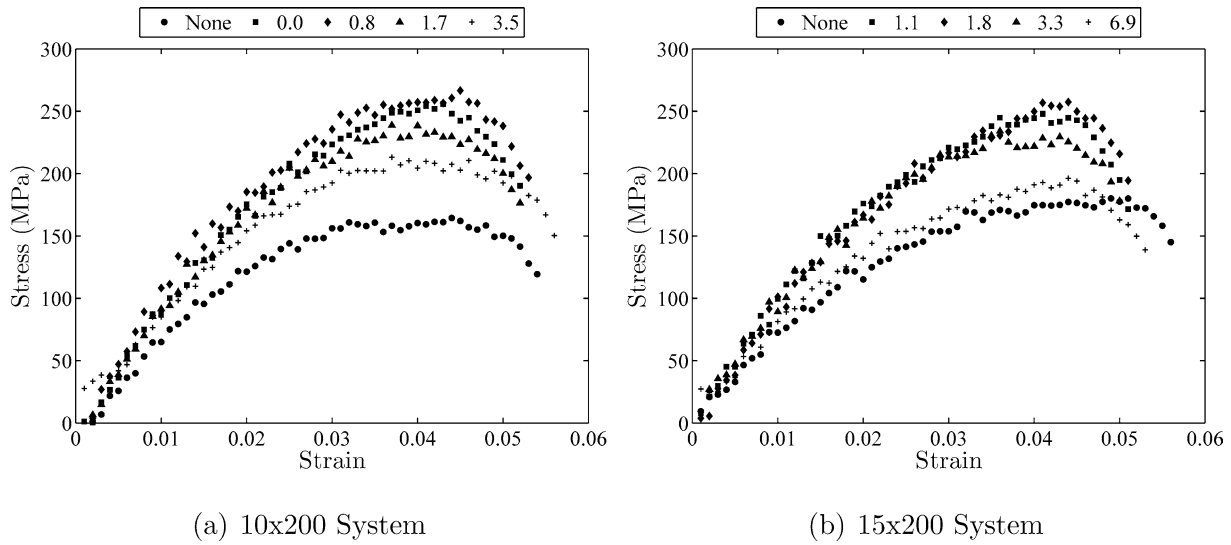

FIGURE 13 Stress-strain curves for the simulations of interface decohesion. Carbon dioxide pressures in MPa are given in the legend.

affine transformation of the deformation. From this measure of stress, the strain energy is calculated as

$$W = \int_0^{\epsilon_f} \boldsymbol{\sigma} : d\boldsymbol{\epsilon} \approx \int_0^{\epsilon_f} \sigma_{33} d\epsilon_{33} \tag{14}$$

Here, $\boldsymbol{\epsilon}$ is the Cauchy strain tensor, and $\boldsymbol{\epsilon}_f$ denotes the strain developed at interface decohesion, where the maximum normal stress σ_{33} is achieved. The strain ϵ_{33} is defined as the ratio $\Delta L/L_0$ of the change of length in the nonperiodic direction to the original length in that direction. It is assumed that the in-plane stresses and strains are significantly smaller than those $(\sigma_{33}, \epsilon_{33})$ in the thickness direction. This measure of strain energy is used as a metric to determine the relative integrity of the interface in each molecular system. Figure 14 demonstrates that the integrity is enhanced by CO_2 pressure conditions up to a maximum at ~2 MPa. Further addition of CO_2 beyond this begins to degrade the integrity of the partially healed interface.

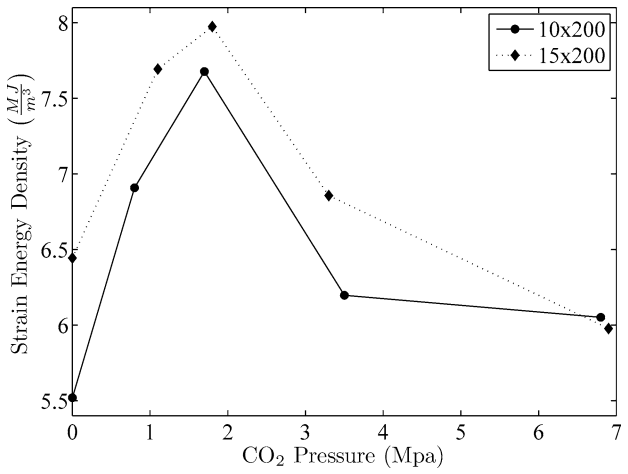

FIGURE 14 Strain energy density developed up to decohesion as a function of CO_2 pressure.

The strain energy density measured for the system consisting of two 10×200 PS films under 1.7 MPa CO_2 is 7.67 MJ/m^3. This is greater than 50% of the value 414.56 MJ/m^3 that is obtained for a virgin 20×200 PS film subjected to similar simulation conditions for decohesion. It points to a significant development of strength. A sensitivity study is performed to test the dependence of the strain energy values on time across the range of MD-accessible simulation times. This study is performed by simulating an interface healing example between two 10×200 films for 0.5, 1.0, 2.0, 3.0, 6.0, and 33.0 ns under no CO_2 and 2 MPa CO_2 pressure conditions respectively, and subsequently testing the decohesion behavior as described above. As shown in Figure 15, there is an initial phase of limited strength development for times less than 1 ns, followed by a rapid development of strength in the 1–3 ns range. This is followed by a final regime of slow strength development

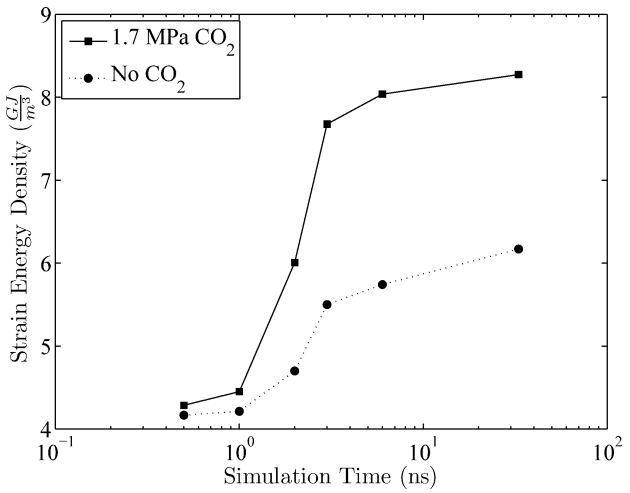

FIGURE 15 Strain energy density developed up to decohesion as a function of simulation time for the 10×200 polymer system under two CO_2 pressure conditions.

beyond 3 ns, continuing to 33 ns. This regime of slow strength development is marked by an increase in the inter-penetration depth, while the other measured values are stable. This is seen as an indication of the initial period of strength development giving way to the longer timescale bond strengthening characterized primarily by the bulk diffusion and interface widening observed in experiments.

CONCLUSIONS

This molecular dynamics based study is intended to investigate the effect of CO_2 on the interface of PS thin films. This property is important in the fabrication of nanoscale film structures by bonding thin films. Simulations of bonding at the thin film interfaces are carried out on 5 and 7 nm thick PS thin films at 300 K. This temperature is below the bulk glass transition temperature T_g^b, but above the surface glass transition temperature T_g^s.[9] This temperature is sufficiently high to allow for limited diffusion of PS chain segments across symmetric interfaces between the thin films. The introduction of increasing pressures of CO_2 is found to affect certain important properties of the polymer at the bonding interface, producing a strong dependence between interface integrity and CO_2 pressure.

Part of this dependence is brought about by two competing trends. First, the average monomer inter-penetration depth is found to increase with increasing CO_2 pressure. This indicates that the introduction of CO_2 facilitates the diffusion of chain segments across the interface, with increasing amounts of diffusion for CO_2 pressures up to $\sim$7 MPa. The inherent limitations on the timescale accessible by MD simulation prevents a detailed study of this important mechanism over its characteristic timescale. However, the extended simulations performed in this study show that the continued increase in inter-penetration is accompanied by an increase in the measured integrity of the film-film interface. Second, the introduction of CO_2 into the polymer systems is found to impact the free volume characteristics of the bonding interface. At elevated pressures of CO_2, free volume cavities at the interface are fewer and larger, and account for a net gain in free volume at the interface. This increase in free volume leads to a greater average separation between the film surfaces for the range of CO_2 pressures investigated up to $\sim$7 MPa. It is found that the changes in free volume characteristics at the interface stabilize within the MD timescale, with no evidence of time-dependence observed in the 3–33 ns range of the two extended simulations that are performed.

The competing mechanisms point to an optimal amount of CO_2 required for a maximum enhancement of adhesive strength at the bonded interface. Much of the strength that is developed is due to the van der Waals attraction between atoms on opposite sides of the thin film interface. Processing in a CO_2 environment facilitates diffusion of atoms across the interface. It increases the surface area of the films at the interface and therefore the number of atoms from opposing films that are in close proximity. This phenomenon enhances the strength of the adhesion at the interface. At the same time, CO_2 enhances the free volume in the polymer. Separation between the film surfaces increases, limiting the strength of the attractive forces that atoms at the film surfaces exert across the interface.

A second source of adhesive strength at the interface is the existence of chemically bonded atoms from molecules in one film, bridging the interfacial gap and penetrating into the opposing film. It is shown that this process is enabled by the enhanced mobility that is maximized under CO_2 pressure conditions in the neighborhood of 2 MPa. As a bridging segment from one film penetrates into the other, the adhesive strength of this bridge approaches the strength of the covalent bonds in the segment. Thus, the energy required to separate the interface at a bridge is potentially much higher than that required to separate the films when the surfaces are held together with the weaker van der Waals attraction between the film surfaces. In fact, increasing the number of bridging segments is demonstrated to be a mechanism for the development of significant adhesive strength, as previously theorized.[43,44] The development of these bridging segments is only observed in the first few nanoseconds of the bonding simulations. Thus, conclusions the conclusions drawn from the trends observed in this quantity with respect to varying CO_2 pressure are expected to remain valid at longer timescales.

This study finds that the strongest adhesion is produced for CO_2 pressure conditions in the neighborhood of 2 MPa in the model systems studied. As the sorption of CO_2 has a negligible affect on the tensile strength[45] and elastic modulus[46] of PS, it is asserted that the observed increase in strength is due to enhancement of the interfacial adhesion. While the exact values of the temperature and CO_2 pressure are almost certainly material- and size-dependent, two main ideas are widely applicable. First, for nanoscale polymer structures, the difference between bulk and surface glass transition temperatures can be exploited to produce viable bonds at a processing temperature $T_g^s < T_p < T_g^b$. Second, the enhancement of adhesive strength at the bonding interface via CO_2 is directly related to the enhancement of chain mobility at the interface, which is maximum at a finite CO_2 pressure.

Lastly, it is noted that the MD timescale prevents the simulation of the complete bonding process. To circumvent this limitation, a careful examination is made of the time-dependence of the quantities investigated to explain the observed trends in adhesive strength with respect to CO_2 pressure. As a result of this analysis, it is expected that the conclusions made based on the results of this study should remain valid even for more realistic timescales.

ACKNOWLEDGMENTS

This work was supported by the NSF Division of Engineering Education & Centers through grant #EEC-0425626 to the Center for Affordable Nanoengineering of Polymeric Biomedical Devices (CANPBD) at the Ohio State University (Professor L. James Lee, Director). This sponsorship is gratefully acknowledged. The authors thank Lee for his advice and support of this project. Computer support by the Ohio Supercomputer Center through grant PAS0191 is also gratefully acknowledged.

REFERENCES AND NOTES

1 Ellis, J., Tomasko, D. L., Dehghani, F. *Biomacromolecules* **2008**, *9*, 1027–1034.

2 Yang, Y., Lui, D., Xie, Y., Lee, L. J., Tomasko, D.L. *Adv. Mater.* **2007**, *19*, 251–254.

3 Chiou, J. S., Barlow, J. W., Paul, D. R. *J. Appl. Polym. Sci.* **1985**, *30*, 2633–2642.

4 Wissinger, R. G., Paulaitis, M. E. *J. Polym. Sci. Part B: Polym. Phys.* **1987**, *25*, 2497–2510.

5 Chen, H., Cheng, M.-L., Jean, Y. C., Lee, L. J., Yang, J. *J. Polym. Sci. Part B: Polym. Phys.* **2008**, *46*, 388–405.

6 Srivastava, A., Alleman, C., Ghosh, S., Lee, L. J. *Model. Simul. Mater. Sci. Eng.* **2010**, *18*, 065003.

7 Spyriouni, T., Boulougouris, G., Theodorou, D. N. *Macromolecules* **2009**, *42*, 1759–1769.

8 Jean, Y. C., Zhang, R., Cao, H., Yuan, J.-P., Huang, C.-M., Nielsen, B., Asoka-Kumar, P. *Phys. Rev. B* **1997**, *56*, R8459–R8462.

9 Satomi, N., Tanaka, K., Takahara, A., Kajiyama, T. *Macromolecules* **2001**, *34*, 8761–8767.

10 Kim, Y. H., Wool, R. P. *Macromolecules* **1983**, *16*, 1115–1120.

11 Karim, A., Mansour, A., Felcher, G. P. *Phys. Rev. B* **1990**, *42*, 6846–6849.

12 Karim, A., Arendt, B. H., Felcher, G. P. *Thin Solid Films* **1991**, *202*, 345–350.

13 Jilge, W., Carmesin, I., Kremer, K., Binder, K. *Macromolecules* **1990**, *23*, 5001–5013.

14 Deutsch, H. P., Binder, K. *J. Chem. Phys.* **1990**, *94*, 2294–2304.

15 Pierce, F., Perahia, D., Grest, G. S. *Macromolecules* **2009**, *42*, 7969–7973.

16 Schnell, R., Stamm, M., Creton, C. *Macromolecules* **1998**, *31*, 2284–2292.

17 Akabori, K.-I., Baba, D., Koguchi, K., Tanaka, K., Nagamura, T. *J. Polym. Sci. Part B: Polym. Phys.* **2006**, *44*, 3598–3604.

18 Brown, H. R. *Macromolecules* **2001**, *34*, 3720–3724.

19 Chaturvedi, U. K., Steiner, U., Zak, O., Krausch, G., Klein, J. *Phys. Rev. Lett.* **1989**, *63*, 616–619.

20 Boiko, Y. M., Prud'homme, R. E. *Macromolecules* **1998**, *31*, 6620–6626.

21 Boiko, Y. M., Bach, A., Lyngaae-Jorgensen, J. *Polym. Sci. Part B: Polym. Phys.* **2004**, *42*, 1861–1867.

22 Zhang, X., Tasaka, S., Inagaki, N. *J. Polym. Sci. Part B: Polym. Phys.* **2000**, *38*, 654–658.

23 Yang, J., Liu, C., Yang, Y., Zhu, B., Lee, L. J., Chen, H., Jean, Y. C. *Polym. Sci. Part B: Polym. Phys.* **2009**, *47*, 1535–1542.

24 Srivastava, A., Ghosh, S. *Int. J. Multiscale Comput. Eng.* **2010**, *8*, 535–547.

25 Wool, R. P. Polymer Interfaces: Structure and Strength; Hanser: New York, 1995.

26 Haire, K. R., Windle, A. H. *Comput. Theor. Polym. Sci.* **2001**, *11*, 227–240.

27 Anderson, K. L., Wescott, J. T., Carver, T. J., Windle, A. H. *Mater. Sci. Eng. A* **2004**, *A365*, 14–24.

28 Wick, C. D., Martin, M. G., Siepmann, J. I. *J. Phys. Chem. B* **2000**, *104*, 8008–8016.

29 Harmandaris, V. A., Adhikari, N. P., van der Vegt, N. F. A., Kremer, K. *Macromolecules* **2006**, *39*, 6708–6719.

30 Han, J., Boyd, R. H. *Polymer* **1996**, *37*, 1797–1804.

31 Harris, J. G., Yung, K. H. *J. Phys. Chem.* **1995**, *99*, 12021–12024.

32 LAMMPS Users Manual, Sandia National Laboratories (2010).

33 Halgren, T. A. *J. Am. Chem. Soc.* **1992**, *114*, 7827–7843.

34 Allen, M. P., Tilsesley, D. J. Computer Simulation of Liquids; Oxford University Press: Oxford, 1987.

35 Wissinger, R. G., Paulaitis, M. E. *J. Polym. Sci. Part B: Polym. Phys.* **1991**, *29*, 631–633.

36 Kawaguchi, D., Tanaka, K., Kajiyama, T. *Macromolecules* **2003**, *36*, 1235–1240.

37 Kawana, S., Jones, R. A. L. *Phys.Rev. E* **2001**, *63*, 021501.

38 Baljon, A. R. C., Williams, S., Balabaev, N. K., Hudzinskyy, D., Lyulin, A. V. *J. Polym. Sci. Part B* **2010**, *48*, 1160–1167.

39 Prager, S., Tirrell, M. *J. Chem. Phys.* **1981**, *75*, 5194–5198.

40 Prince E. Rouse, Jr. *J. Chem. Phys.* **1953**, *21*, 1272–1280.

41 Tsai, D. H. *J. Chem. Phys.* **1979**, *70*, 1375–1382.

42 Admal, N. C., Tadmor, E. B. *J. Elasticity* **2010**, *100*, 63–143.

43 Raphael, E., de Gennes, P. G. *J. Phys. Chem.* **1992**, *96*, 4002–4007.

44 Ji, H., de Gennes, P. G. *Macromolecules* **1993**, *26*, 520–525.

45 Jiménez, A., Thompson, G. L., Matthews, M. A., Davis, T. A., Crocker, K., Lyons, J. S., Trapotsis, A. *J. Supercrit. Fluids* **2007**, *42*, 366–372.

46 Wang, W.-C. V., Kramer, E. J., Sachse, W. H. *J. Polym. Sci.: Polym. Phys. Ed.* **1982**, *20*, 1371–1384.